Progress In Electromagnetics Research, Vol. 116, 553–567, 2011

A NEW WIDE-STOPBAND LOW-PASS FILTER WITH GENERALIZED COUPLED-LINE CIRCUIT AND ANALYTICAL THEORY

Y. Wu*, Y. Liu, S. Li, and C. Yu

School of Electronic Engineering, Beijing University of Posts and Telecommunications, Beijing, China

Abstract—A generalized coupled-line circuit is introduced to construct a wide-stopband low-pass filter in this paper. This circuit configuration includes two-section coupled lines and a connected transmission-line stub. Due to the symmetry of this proposed structure, closed-form equations for scattering parameters are investigated. The transmission zeros and poles locations for different circuit parameters are discussed, and the corresponding design curves are given. For theoretical verifications, four typical numerical examples are designed, calculated and illustrated. Furthermore, two single-stage low-pass filters (LPF 1 and LPF 2) with the 1-dB cutoff frequencies of 0.72 GHz and 1.45 GHz are fabricated and measured. The implemented LPF 2 has 19-dB stopband rejection in the range of 2.05 to 6.36 GHz. Finally, two LPF cells (LPF 1 and LPF 2) and an additional connected transmission line are used to construct a new two-stage low-pass filter (LPF 3) with extended stopband. The measured 16-dB stopband of LPF 3 is up to 7.5 GHz while the 1-dB passband range is from DC to 0.67 GHz. The advantages of this proposed low-pass filter are avoiding any lumped elements and compact layout structure.

1. INTRODUCTION

With the rapid development of the advanced RF/Microwave wireless communication systems, many planar filters [1–6] with band-pass, low-pass, or band-stop performances have been received wide attention, recently. As a kind of fundamental components, high-performance low-pass filters (LPFs) with low insertion loss, sharp rejection, wide stopband, compact size, and flexible reconfiguration are highly required

Received 10 April 2011, Accepted 19 May 2011, Scheduled 24 May 2011

* Corresponding author: Yongle Wu (wuyongle138@gmail.com).

in modern communication systems. Most LPFs are usually used to suppress the unwanted signals including spurious and harmonics. Due to usage of high-performance low-cost LPFs, the linearity of the main RF front-end can be improved and the bit error rate (BER) of the wireless communication systems can be reduced [7, 8]. The most conventional techniques for implementing LPFs are employing stepped-impedance structure and open-stub circuit [7]. However, these single-stage stepped-impedance or open-stub LPFs suffer from gradual cutoff response and narrow stopband [7].

In order to improve performances of LPFs, several techniques for designing LPFs have been explored in [9–24]. The proposed harmonic-rejection LPF in [9] includes a transmission line section and a coupled line section. This new single-stage LPF have three attenuation poles in the stop band. Sheen has employed a semi-lumped parallel resonance circuit to design a novel low-pass filter in [10], and this filter has two finite attenuation poles which improve the performance of stopband. In addition, instead of a lumped capacitor in [10], an interdigital capacitor has been used to design a compact distributed LPF in [11]. Microstrip stepped-impedance hairpin resonators are useful to design high-performance LPF because the advantages of compact size and easy implementation, as discussed in [12–14]. The defected ground structure (DGS) with different circuit layouts has been developed to design many kinds of LPFs in [15–18]. Actually, the used complementary split ring resonators in [18] can be considered as a kind of DGS. The key disadvantages of DGS include the additional radiation from the partially open ground and requiring the complicated wasting-time electromagnetic simulation. The proposed compact resonators in [19, 20] can be applied to design compact, wide-stopband LPFs. However, the corresponding analytical theories cannot easily be achieved due to circuit layouts' complexity. As a new research direction, the offset finite-ground microstrip line with narrow strip or ground width can also be investigated to construct harmonic-suppressed LPFs, as studied in [21]. Different from the above-mentioned design structures or methods, the anti-coupled line with open-circuited resonator (lumped capacitive load or radial stubs) has been proposed to construct LPFs with improved stopband characteristics [22–24] and wideband bandstop filters [25]. Furthermore, by introducing additional terminated coupled-line section into anti-coupled line, a novel bandpass filter with analytical design theory has been developed in [26]. Therefore, it is confirmed that anti-coupled line is a simple and effective circuit configuration for microstrip filters.

In this paper, a new coupled-line circuit is proposed to construct

a novel low-pass filter. This investigated circuit configuration is composed of two-section coupled lines and a connected transmission-line stub. Since the total circuit layout is based on coupled lines, which is symmetrical and simple, this LPF not only has analytical scattering parameters' expressions, but also features compact size and flexible reconfiguration. This proposed circuit is generalized because the previous structures in both [13] and [22] are special cases of this paper. Furthermore, based on the obtained equations, the design curves for transmission zeros and poles locations are illustrated when different circuit parameters are employed. Then, four numerical examples are presented for theoretical verifications. In addition, two single-stage microstrip LPFs (LPF 1 and LPF 2) with the 1-dB cutoff frequencies of 0.72 GHz and 1.45 GHz are designed, fabricated and measured. The implemented LPF 1 (LPF 2) has 19-dB stopband rejection in the range of 1.04 GHz to 3.2 GHz (2.05 GHz to 6.36 GHz). Finally, a two-stage microstrip LPF (LPF 3) is achieved by using two LPF cells (LPF 1 and LPF 2) and an additional connected transmission line. The 16-dB stopband of the measured LPF 3 is further extended to 7.5 GHz.

2. THE CIRCUIT STRUCTURE AND THEORY OF THE PROPOSED LPF

The proposed LPF's circuit structure is illustrated in Fig. 1. This novel structure consists of two-section coupled lines (Z_{ie}, Z_{io}, $i = 1, 2$) and an open-circuit transmission-line stub (Z_3). These coupled lines and the open-circuit stub are connected at the point P, as shown in Fig. 1(a). Two port impedances are chosen as Z_o. Since the total

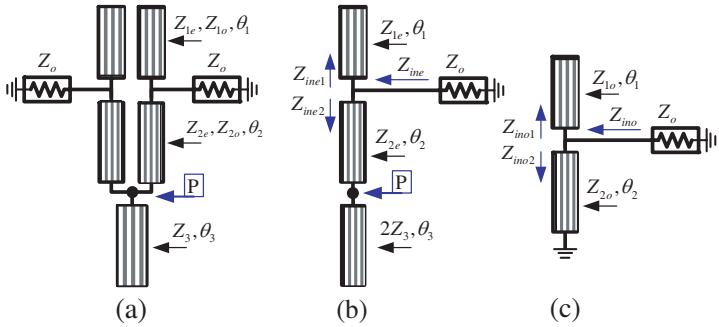

Figure 1. The proposed LPF's circuit structure: (a) Total circuit configuration, (b) half circuit under even-mode excitation, (c) half circuit under odd-mode excitation.

circuit configuration shown in Fig. 1(a) is symmetrical, this model's scattering parameters can be analyzed through using the even- and odd-mode method [7]. Figs. 1(b) and (c) show the even- and odd-mode equivalent circuits of the total circuit configuration in Fig. 1(a), respectively.

According to the symmetrical network analysis results [7, 26], the network analysis of Fig. 1(a) will be simplified by analyzing the one-port networks shown in Figs. 1(b) and (c). In other words, if the one-port, even- and odd-mode scattering parameters S_{11e} and S_{11o} are obtained, the two-port scattering parameters of Fig. 1(a) can be calculated as

$$S_{11} = \frac{S_{11e} + S_{11o}}{2}, \quad S_{21} = \frac{S_{11e} - S_{11o}}{2}. \tag{1}$$

Two groups of input equivalent impedances including Z_{ine}, Z_{ine1}, Z_{ine2}, Z_{ino}, Z_{ino1}, and Z_{ino2} are defined in the Figs. 1(b) and (c). For Fig. 1(b), their mathematical expressions can be obtained as

$$Z_{ine1} = \frac{-jZ_{1e}}{\tan(\theta_1)}, \tag{2a}$$

$$Z_{ine2} = jZ_{2e}\frac{Z_{2e}\tan(\theta_2)\tan(\theta_3) - 2Z_3}{Z_{2e}\tan(\theta_3) + 2Z_3\tan(\theta_2)}. \tag{2b}$$

The total input equivalent impedance Z_{ine} is calculated by using the following equation

$$Z_{ine} = \frac{Z_{ine1}Z_{ine2}}{Z_{ine1} + Z_{ine2}}. \tag{3a}$$

Thus, the final result is expressed by

$$Z_{ine} = j\frac{Z_{1e}Z_{2e}[Z_{2e}\tan(\theta_2)\tan(\theta_3) - 2Z_3]}{\begin{array}{l}Z_{1e}[Z_{2e}\tan(\theta_3) + 2Z_3\tan(\theta_2)] \\ -Z_{2e}\tan(\theta_1)[Z_{2e}\tan(\theta_2)\tan(\theta_3) - 2Z_3]\end{array}}. \tag{3b}$$

Similarly, For Fig. 1(c), the odd-mode input equivalent impedances can be derived as

$$Z_{ino1} = \frac{-jZ_{1o}}{\tan(\theta_1)}, \quad Z_{ino2} = jZ_{2o}\tan(\theta_2), \tag{4}$$

The final odd-mode input impedance Z_{ino} can be obtained as

$$Z_{ino} = \frac{Z_{ino1}Z_{ino2}}{Z_{ino1} + Z_{ino2}} = j\frac{Z_{1o}Z_{2o}\tan(\theta_2)}{Z_{1o} - Z_{2o}\tan(\theta_1)\tan(\theta_2)}. \tag{5}$$

Thus, the reflection coefficients S_{11e} and S_{11o} for Figs. 1(b) and (c) can be calculated by

$$S_{11k} = \frac{Z_{ink} - Z_o}{Z_{ink} + Z_o}, k = o, e. \tag{6}$$

After some straightforward manipulation, the expressions of S_{11e} and S_{11o} are given by

$$S_{11e} = \frac{\begin{pmatrix} jZ_{1e}Z_{2e}[Z_{2e}\tan(\theta_2)\tan(\theta_3) - 2Z_3] \\ -Z_o\{Z_{1e}[Z_{2e}\tan(\theta_3) + 2Z_3\tan(\theta_2)] \\ -Z_{2e}\tan(\theta_1)[Z_{2e}\tan(\theta_2)\tan(\theta_3) - 2Z_3]\} \end{pmatrix}}{\begin{pmatrix} jZ_{1e}Z_{2e}[Z_{2e}\tan(\theta_2)\tan(\theta_3) - 2Z_3] \\ +Z_o\{Z_{1e}[Z_{2e}\tan(\theta_3) + 2Z_3\tan(\theta_2)] \\ -Z_{2e}\tan(\theta_1)[Z_{2e}\tan(\theta_2)\tan(\theta_3) - 2Z_3]\} \end{pmatrix}}, \tag{7a}$$

$$S_{11o} = \frac{jZ_{1o}Z_{2o}\tan(\theta_2) - Z_o[Z_{1o} - Z_{2o}\tan(\theta_1)\tan(\theta_2)]}{jZ_{1o}Z_{2o}\tan(\theta_2) + Z_o[Z_{1o} - Z_{2o}\tan(\theta_1)\tan(\theta_2)]}. \tag{7b}$$

Based on combining (1) and (7), the analytical mathematical equations for the LPF in Fig. 1(a) can be simplified as

$$\begin{cases} S_{11} = R_{S_{11}} + jX_{S_{11}} \\ S_{21} = R_{S_{21}} + jX_{S_{21}} \end{cases}, \tag{8a}$$

where

$$R_{S_{11}} = -\frac{1}{2}\left\{ \frac{\begin{pmatrix} \{Z_oZ_{1e}[Z_{2e}\tan(\theta_3) + 2Z_3\tan(\theta_2)] \\ -Z_oZ_{2e}\tan(\theta_1)[Z_{2e}\tan(\theta_2)\tan(\theta_3) - 2Z_3]\}^2 \\ -\{Z_{1e}Z_{2e}[Z_{2e}\tan(\theta_2)\tan(\theta_3) - 2Z_3]\}^2 \end{pmatrix}}{\begin{pmatrix} \{Z_oZ_{1e}[Z_{2e}\tan(\theta_3) + 2Z_3\tan(\theta_2)] \\ -Z_oZ_{2e}\tan(\theta_1)[Z_{2e}\tan(\theta_2)\tan(\theta_3) - 2Z_3]\}^2 \\ +\{Z_{1e}Z_{2e}[Z_{2e}\tan(\theta_2)\tan(\theta_3) - 2Z_3]\}^2 \end{pmatrix}} + \frac{\{Z_o[Z_{1o} - Z_{2o}\tan(\theta_1)\tan(\theta_2)]\}^2 - [Z_{1o}Z_{2o}\tan(\theta_2)]^2}{\{Z_o[Z_{1o} - Z_{2o}\tan(\theta_1)\tan(\theta_2)]\}^2 + [Z_{1o}Z_{2o}\tan(\theta_2)]^2} \right\}, \tag{8b}$$

$$X_{S_{11}} = Z_o\left\{ \frac{\begin{pmatrix} Z_{1e}Z_{2e}[Z_{2e}\tan(\theta_2)\tan(\theta_3) - 2Z_3] \\ \{Z_{1e}[Z_{2e}\tan(\theta_3) + 2Z_3\tan(\theta_2)] \\ -Z_{2e}\tan(\theta_1)[Z_{2e}\tan(\theta_2)\tan(\theta_3) - 2Z_3]\} \end{pmatrix}}{\begin{pmatrix} \{Z_{1e}Z_{2e}[Z_{2e}\tan(\theta_2)\tan(\theta_3) - 2Z_3]\}^2 \\ +\{Z_oZ_{1e}[Z_{2e}\tan(\theta_3) + 2Z_3\tan(\theta_2)] \\ -Z_oZ_{2e}\tan(\theta_1)[Z_{2e}\tan(\theta_2)\tan(\theta_3) - 2Z_3]\}^2 \end{pmatrix}} + \frac{Z_{1o}Z_{2o}\tan(\theta_2)[Z_{1o} - Z_{2o}\tan(\theta_1)\tan(\theta_2)]}{[Z_{1o}Z_{2o}\tan(\theta_2)]^2 + \{Z_o[Z_{1o} - Z_{2o}\tan(\theta_1)\tan(\theta_2)]\}^2} \right\}, \tag{8c}$$

$$R_{S_{21}} = -\frac{1}{2}\left\{ \frac{\begin{pmatrix} \{Z_oZ_{1e}[Z_{2e}\tan(\theta_3) + 2Z_3\tan(\theta_2)] \\ -Z_oZ_{2e}\tan(\theta_1)[Z_{2e}\tan(\theta_2)\tan(\theta_3) - 2Z_3]\}^2 \\ -\{Z_{1e}Z_{2e}[Z_{2e}\tan(\theta_2)\tan(\theta_3) - 2Z_3]\}^2 \end{pmatrix}}{\begin{pmatrix} \{Z_oZ_{1e}[Z_{2e}\tan(\theta_3) + 2Z_3\tan(\theta_2)] \\ -Z_oZ_{2e}\tan(\theta_1)[Z_{2e}\tan(\theta_2)\tan(\theta_3) - 2Z_3]\}^2 \\ +\{Z_{1e}Z_{2e}[Z_{2e}\tan(\theta_2)\tan(\theta_3) - 2Z_3]\}^2 \end{pmatrix}} - \frac{\{Z_o[Z_{1o} - Z_{2o}\tan(\theta_1)\tan(\theta_2)]\}^2 - [Z_{1o}Z_{2o}\tan(\theta_2)]^2}{\{Z_o[Z_{1o} - Z_{2o}\tan(\theta_1)\tan(\theta_2)]\}^2 + [Z_{1o}Z_{2o}\tan(\theta_2)]^2} \right\}, \tag{8d}$$

$$X_{S_{21}} = Z_o \left\{ \begin{array}{l} \dfrac{\left(\begin{array}{c} Z_{1e}Z_{2e}[Z_{2e}\tan(\theta_2)\tan(\theta_3) - 2Z_3] \\ \{Z_{1e}[Z_{2e}\tan(\theta_3) + 2Z_3\tan(\theta_2)] \\ -Z_{2e}\tan(\theta_1)[Z_{2e}\tan(\theta_2)\tan(\theta_3) - 2Z_3]\} \end{array} \right)}{\left(\begin{array}{c} \{Z_{1e}Z_{2e}[Z_{2e}\tan(\theta_2)\tan(\theta_3) - 2Z_3]\}^2 \\ +\{Z_oZ_{1e}[Z_{2e}\tan(\theta_3) + 2Z_3\tan(\theta_2)] \\ -Z_oZ_{2e}\tan(\theta_1)[Z_{2e}\tan(\theta_2)\tan(\theta_3) - 2Z_3]\}^2 \end{array} \right)} \\ -\dfrac{Z_{1o}Z_{2o}\tan(\theta_2)[Z_{1o} - Z_{2o}\tan(\theta_1)\tan(\theta_2)]}{[Z_{1o}Z_{2o}\tan(\theta_2)]^2 + \{Z_o[Z_{1o} - Z_{2o}\tan(\theta_1)\tan(\theta_2)]\}^2} \end{array} \right\}. \quad (8e)$$

Therefore, the external scattering parameters performance (including magnitude and phase information) of the proposed LPF shown in Fig. 1(a) can be calculated and analyzed by using the Equation (8).

3. CHARACTERISTICS OF THE PROPOSED LPF

An ideal low-pass filter property can be described by using the rigorous relationships including $S_{11} = 0$ for the low frequencies and $S_{21} = 0$ for the high frequencies. If $S_{11} = 0$ is considered, the corresponding rigorous equation can be written as

$$\begin{aligned} & \frac{\{Z_o[Z_{1o} - Z_{2o}\tan(\theta_1)\tan(\theta_2)]\}^2 + [Z_{1o}Z_{2o}\tan(\theta_2)]^2}{\left(\begin{array}{l} \{Z_oZ_{1e}[Z_{2e}\tan(\theta_3) + 2Z_3\tan(\theta_2)] \\ -Z_oZ_{2e}\tan(\theta_1)[Z_{2e}\tan(\theta_2)\tan(\theta_3) - 2Z_3]\}^2 \\ +\{Z_{1e}Z_{2e}[Z_{2e}\tan(\theta_2)\tan(\theta_3) - 2Z_3]\}^2 \end{array} \right)} \\ = & -\frac{\{Z_o[Z_{1o} - Z_{2o}\tan(\theta_1)\tan(\theta_2)]\}^2 - [Z_{1o}Z_{2o}\tan(\theta_2)]^2}{\left(\begin{array}{l} \{Z_oZ_{1e}[Z_{2e}\tan(\theta_3) + 2Z_3\tan(\theta_2)] \\ -Z_oZ_{2e}\tan(\theta_1)[Z_{2e}\tan(\theta_2)\tan(\theta_3) - 2Z_3]\}^2 \\ -\{Z_{1e}Z_{2e}[Z_{2e}\tan(\theta_2)\tan(\theta_3) - 2Z_3]\}^2 \end{array} \right)} \\ = & -\frac{Z_{1o}Z_{2o}\tan(\theta_2)[Z_{1o} - Z_{2o}\tan(\theta_1)\tan(\theta_2)]}{\left(\begin{array}{l} Z_{1e}Z_{2e}[Z_{2e}\tan(\theta_2)\tan(\theta_3) - 2Z_3]\{Z_{1e}[Z_{2e}\tan(\theta_3) \\ +2Z_3\tan(\theta_2)] - Z_{2e}\tan(\theta_1)[Z_{2e}\tan(\theta_2)\tan(\theta_3) - 2Z_3]\} \end{array} \right)}. \quad (9) \end{aligned}$$

In addition, if $S_{21} = 0$ is considered, the mathematical expression can be simplified as

$$\begin{aligned} & \frac{\{Z_o[Z_{1o} - Z_{2o}\tan(\theta_1)\tan(\theta_2)]\}^2 + [Z_{1o}Z_{2o}\tan(\theta_2)]^2}{\left(\begin{array}{l} \{Z_oZ_{1e}[Z_{2e}\tan(\theta_3) + 2Z_3\tan(\theta_2)] \\ -Z_oZ_{2e}\tan(\theta_1)[Z_{2e}\tan(\theta_2)\tan(\theta_3) - 2Z_3]\}^2 \\ +\{Z_{1e}Z_{2e}[Z_{2e}\tan(\theta_2)\tan(\theta_3) - 2Z_3]\}^2 \end{array} \right)} \\ = & \frac{\{Z_o[Z_{1o} - Z_{2o}\tan(\theta_1)\tan(\theta_2)]\}^2 - [Z_{1o}Z_{2o}\tan(\theta_2)]^2}{\left(\begin{array}{l} \{Z_oZ_{1e}[Z_{2e}\tan(\theta_3) + 2Z_3\tan(\theta_2)] \\ -Z_oZ_{2e}\tan(\theta_1)[Z_{2e}\tan(\theta_2)\tan(\theta_3) - 2Z_3]\}^2 \\ -\{Z_{1e}Z_{2e}[Z_{2e}\tan(\theta_2)\tan(\theta_3) - 2Z_3]\}^2 \end{array} \right)} \end{aligned}$$

$$= \frac{Z_{1o}Z_{2o}\tan(\theta_2)[Z_{1o} - Z_{2o}\tan(\theta_1)\tan(\theta_2)]}{\begin{pmatrix} Z_{1e}Z_{2e}[Z_{2e}\tan(\theta_2)\tan(\theta_3) - 2Z_3]\{Z_{1e}[Z_{2e}\tan(\theta_3)+2Z_3\tan(\theta_2)] \\ -Z_{2e}\tan(\theta_1)[Z_{2e}\tan(\theta_2)\tan(\theta_3) - 2Z_3]\} \end{pmatrix}}. \quad (10)$$

In the following numerical and experimental examples, electrical lengths of coupled lines and transmission lines are all specified at 2 GHz. Furthermore, we define four special frequencies including f_P, f_{S1}, f_{S2}, and f_{S3}. The frequency point f_P is the reflection zero in the low frequency pass band and its value will be nonzero. The frequency point f_{Si} $(i = 1, 2, 3)$ corresponds to the ith transmission zeros. For clarity, the illustration about these four special frequencies will be presented in the simulated scattering parameters (Example A in Fig. 3). Fig. 2 shows the performance variation of this proposed LPF when different electrical characteristic impedances or electrical lengths are adopted. As shown in Figs. 2(a) and (b), the stop-band frequency point f_{S2} monotonically decreases as θ_1 and θ_2 increases. However, the reverse phenomenon can be observed in Fig. 2(c). Totally, the variation trend for both f_P and f_{S3} is not obvious in Figs. 2(d)–(h). It is very interesting that the special frequencies f_{S1} and f_{S2} will move closer

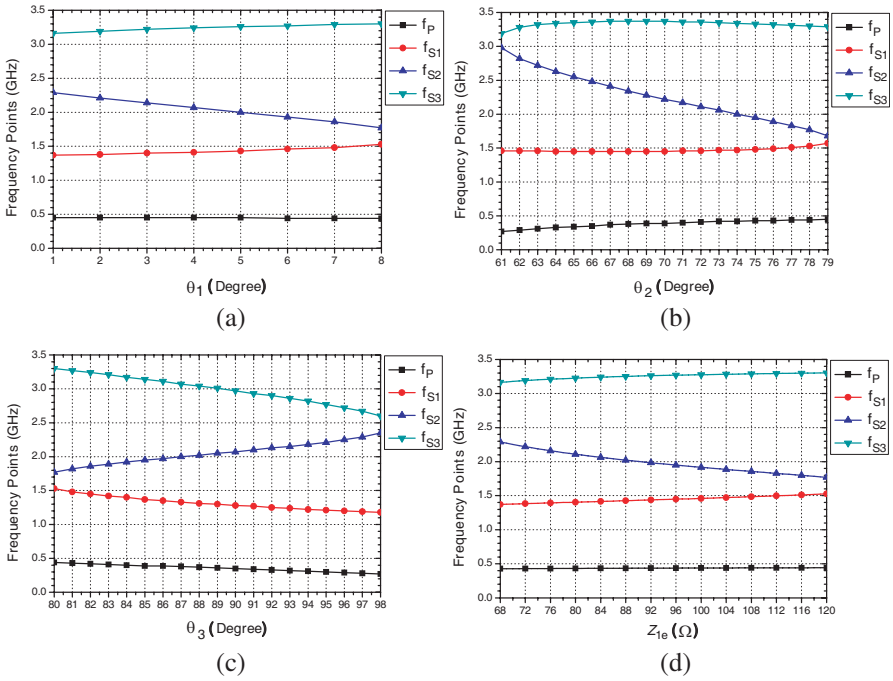

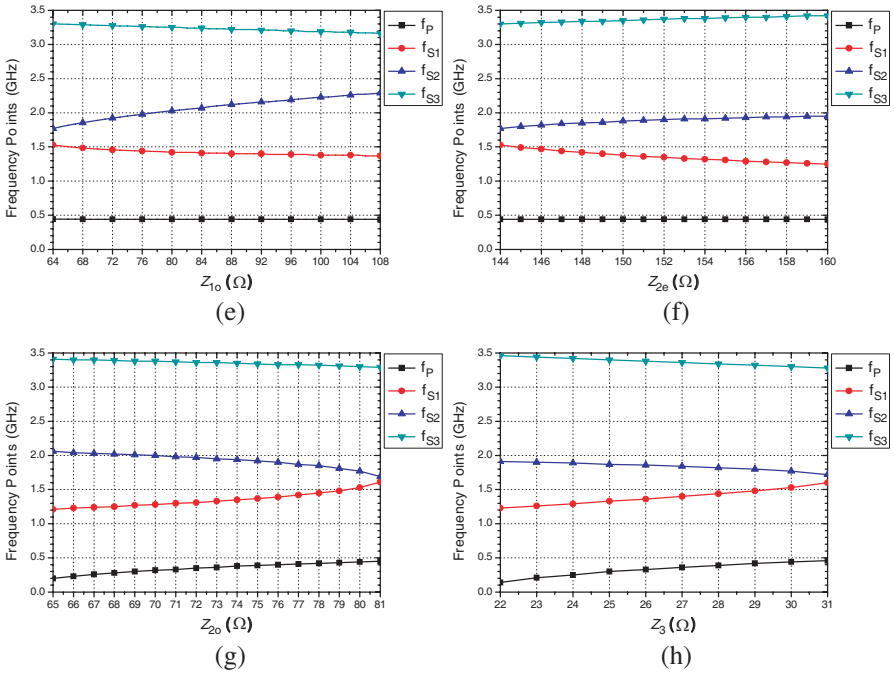

Figure 2. The defined frequency points ***vs*** different electrical parameters including (a) θ_1, (b) θ_2, (c) θ_3, (d) Z_{1e}, (e) Z_{1o}, (f) Z_{2e}, (g) Z_{2o}, and (h) Z_3.

as Z_{2o} increases, as presented in Fig. 2(g). Since different electrical parameters respond to different special frequency points f_P, f_{S1}, f_{S2}, and f_{S3}, it is very difficult to determinate a unique design synthesis method for this novel LPF. The chosen electrical parameters for Fig. 2 are listed in Table 1.

Four numerical examples are designed and calculated. The achieved simulated results shown in Fig. 3 are based on ideal and lossless coupled-line and transmission-line circuit models. The parameters' values for these four examples (Examples A–D) are neglected, since the similar electrical parameters are listed in Table 1. As shown in Fig. 3(a), the 1-dB cutoff frequency of Example A is 0.73 GHz while the first zero f_{S1} of Example A is 1.37 GHz. The reflection zero f_P of Example A is 0.43 GHz, which is close to the stopband. Therefore, shirt selectivity of Example A is relatively obvious. For Examples B and C, the second transmission zero f_{S2} decreases to lower than 2 GHz, as shown in Figs. 3(b) and (c). Thus, the 20-dB rejection level cannot be kept in the total

Table 1. The electrical parameters' values for Fig. 2 ($Z_o = 50\ \Omega$).

Figures	Fig. 2(a)	(b)	(c)	(d)	(e)	(f)	(g)	(h)
θ_1 (Degree)	$1 \sim 8$	8	8	8	8	8	8	8
θ_2	78	61–79	78	78	78	78	78	78
θ_3	80	80	80–98	80	80	80	80	80
Z_{1e} (Ω)	120	120	120	68–120	120	120	120	120
Z_{1o}	64	64	64	64	64–108	64	64	64
Z_{2e}	150	150	150	150	150	144–160	150	150
Z_{2o}	80	80	80	80	80	80	65–81	80
Z_3	30	30	30	30	30	30	30	22–31

stopband, such as from 1.1 to 3.52 GHz for Example B. In this stopband, the maximum transmission parameter $|S_{21}|$ of Example B is about -18.4 dB. Compared to Example B, the pass-band feature of Example C (lower than -30 dB) is relatively improved. The magnitude performance of Example D is very similar to Example A. However, as shown in Fig. 3(e), the group delay of Example D is larger than that of Example A, especially in the relatively high frequency (near 0.5 GHz).

4. MICROSTRIP EXAMPLES AND MEASUREMENTS

In order to experimentally verify the proposed low-pass filters, three LPFs are designed, fabricated, and measured. Firstly, two single-stage LPFs (LPF 1 and LPF 2) are chosen as two typical examples, the design parameters' values and circuit structures are shown in Fig. 4. To extend the stop-band range of this novel LPF, the LPF 1 and LPF 2 are cascaded to form a two-order filter with improved rejection depth.

The calculated scattering parameters of LPFs 1–3 are compared in Figs. 5(a) and (b). Obviously, compared to LPF 1, the 1-dB cutoff frequency of LPF 2 is larger due to the smaller electrical lengths in circuit models. The theoretical pass-band return loss (RL) from DC to 0.55 GHz (1.1 GHz) is better than 20 dB for LPF 1 (LPF 2), as shown in Fig. 5(a). The calculated insertion loss (IL) is better than 1 dB in DC-0.72 GHz (DC-1.45 GHz) and better than 2 dB from DC-0.78 GHz (DC-1.56 GHz) for LPF 1 (LPF 2). The most important is that the stop-band from 1.16 GHz to 6.57 GHz has 20-dB rejection level for the calculated LPF 3. These designed coupled-line LPFs have been fabricated by using microstrip technology on the Rogers R04350B Substrate ($\varepsilon_r = 3.48$ and $h = 0.762$ mm). The practical

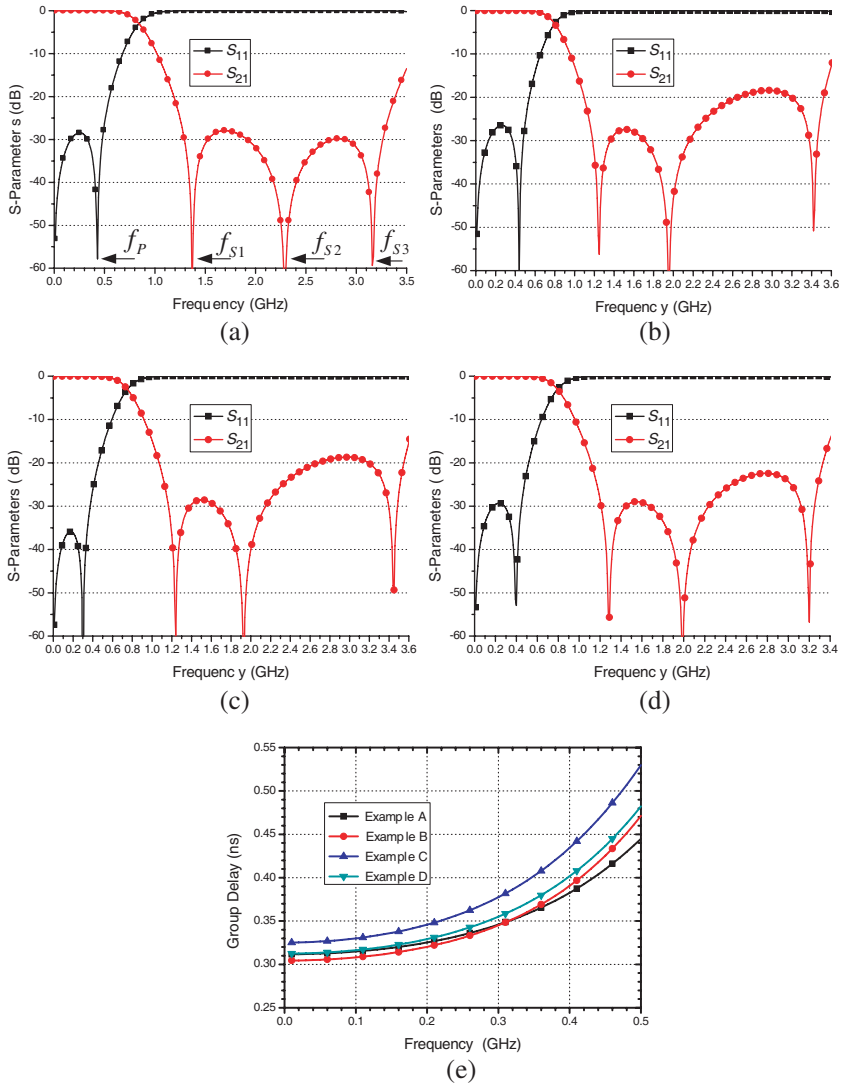

Figure 3. (a)–(d) The simulated scattering parameters of four numerical LPFs and (e) their group delay comparison.

layouts of three microstrip LPFs are shown in Fig. 5(c). The strip width and space width of the first coupled line (second) are 0.5 mm and 0.3 mm (0.28 mm and 0.34 mm), respectively. The measured scattering parameters are obtained from the Agilent N5230C Network Analyzer. As shown in Figs. 6(a) and (b), the measured insertion loss in the range of DC to 0.65 GHz (DC to 1.25 GHz) for LPF 1 (LPF 2) is

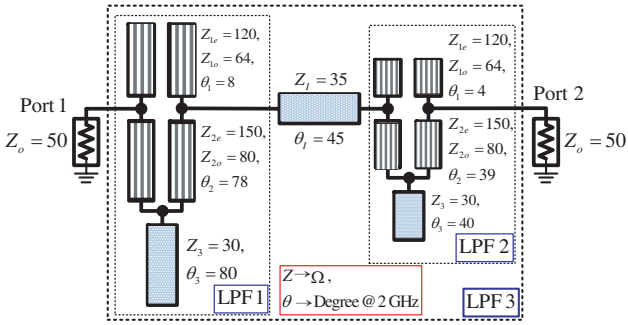

Figure 4. The considered LPFs 1–3 circuit model with accurate electrical parameters' values.

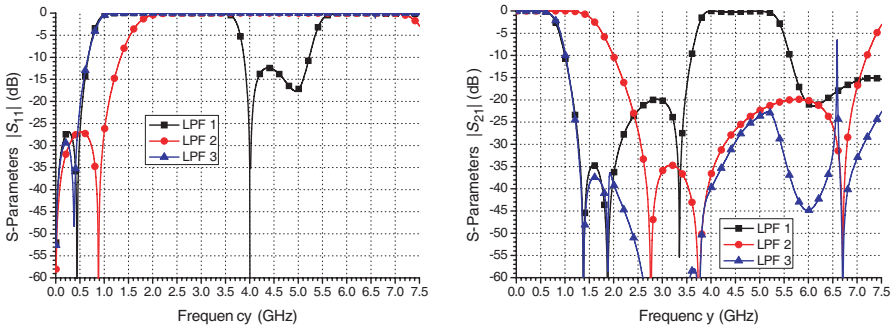

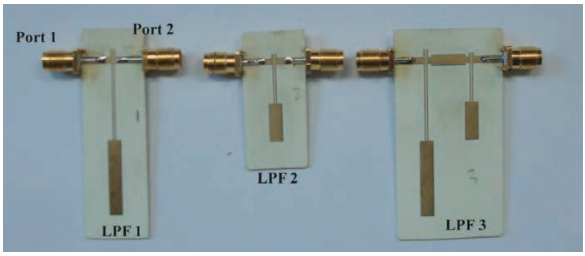

(c)

Figure 5. The calculated scattering parameters of LPFs 1–3 ((a) reflection coefficient, (b) transmission feature) and (c) the photograph of these three LPFs.

better than 1 dB while the measured attenuation poles for LPF 1 (LPF 2) are 1.15 GHz, 2.16 GHz, and 3.08 GHz (2.33 GHz, 3.65 GHz, and 6.16 GHz). The measured results for LPF 3 are shown in Fig. 6(c). It is shown that 16-dB suppression of the fabricated LPF 3 can extend

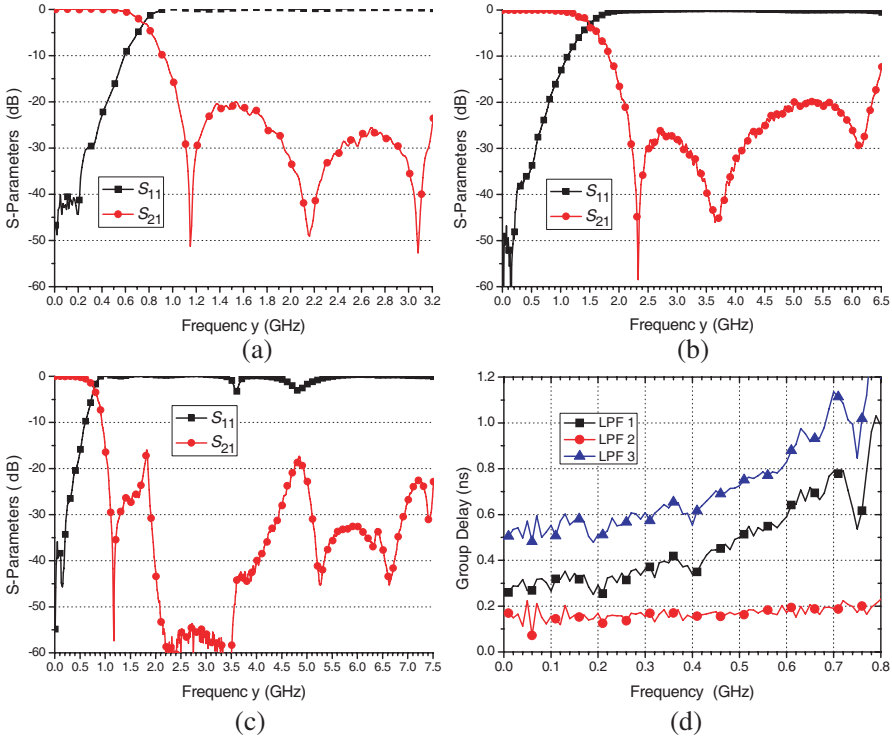

Figure 6. The measured scattering parameters of LPFs 1–3 ((a) LPF 1; (b) LPF 2; (c) LPF 3) and the measured group delay comparison of these three fabricated LPFs.

over 7.5 GHz. The 30-dB suppression band is in the range of 1.91 GHz to 4.44 GHz, as shown in Fig. 6(c). The group delay comparison for three LPFs 1–3 are presented in Fig. 6(d), it is shown that the measured group delay variation in the band of DC to 0.4 GHz is smaller than 0.2 ns. In general, these low-pass filters have good measured transition response and wide-band suppression with high level.

5. CONCLUSION

A simple and symmetrical coupled-line structure is proposed to design a novel microstrip low-pass filter. The rigorous theoretical analysis and complete numerical simulation are discussed. The demonstrated reflection and transmission zeros character may be helpful to guide the synthesis of this proposed LPF. Four numerical examples and three fabricated microstrip LPFs verify our proposed idea. The measured

results show a good agreement with the predicted performance. This LPF has several advantages including compact size, analytical scattering parameters, low insertion loss, high suppression level, avoiding any lumped elements, easy implementation and good group delay.

ACKNOWLEDGMENT

This work was supported in part by Important National Science & Technology Specific Projects (No. 2010ZX03007-003-04), National Natural Science Foundation of China (No. 61001060), and BUPT Excellent Ph.D. Students Foundation (CX201021).

REFERENCES

1. Yu, W.-H., J. Mou, X. Li, and X. Lv, "A compact filter with sharp-transition and wideband-rejection using the novel defected ground structure," *Journal of Electromagnetic Waves and Applications*, Vol. 23, No. 2–3, 329–340, 2009.
2. Wang, J. P., L. Wang, Y.-X. Guo, Y. X. Wang, and D. Fang, "Miniaturized dual-mode bandpass filter with controllable harmonic response for dual-band applications," *Journal of Electromagnetic Waves and Applications*, Vol. 23, No. 11–12, 1525–1533, 2009.
3. Yang, M., J. Xu, Q. Zhao, and X. Sun, "Wide-stopband and miniarurized lowpass filters using sirs-loaded hairpin resonators," *Journal of Electromagnetic Waves and Applications*, Vol. 23, No. 17–18, 2385–2396, 2009.
4. Dai, G. and M. Xia, "An investigation of quarter-wavelength square-spiral resonator and its applications to miniaturized bandpass filters," *Journal of Electromagnetic Waves and Applications*, Vol. 24, No. 10, 1303–1313, 2010.
5. Lin, H.-J., X.-Q. Chen, X.-W. Shi, L. Chen, and C.-L. Li, "A dual passband filter using hybrid microstrip open loop resonators and coplanar waveguide slotline resonators," *Journal of Electromagnetic Waves and Applications*, Vol. 24, No. 1, 141–149, 2010.
6. Chen, H., Y.-H. Wu, Y.-M. Yang, and Y.-X. Zhang, "A novel and compact bandstop filter with folded microstrip/cpw hybrid structure," *Journal of Electromagnetic Waves and Applications*, Vol. 24, No. 1, 103–112, 2010.
7. Hong, J.-S. and M. J. Lancaster, *Microstrip Filters for*

RF/Microwave Applications, Chapters 2 and 5, Wiley, New York, 2001.

8. Cameron, R. J., C. M. Kudsia, and R. R. Mansour, *Microwave Filters for Communication Systems: Fundamentals, Design and Applications*, John Wiley & Sons, Hoboken, NJ, 2007.
9. Lee, Y.-W., S.-M. Cho, G.-Y. Kim, J.-S. Park, D. Ahn, and J.-B. Lim, "A design of the harmonic rejection coupled line low-pass filter with attenuation poles," *Asia Pacific Microwave Conference*, Vol. 3, 682–685, 1999.
10. Sheen, J. W., "A compact semilumped low-pass filter for harmonics and spurious suppression," *IEEE Microwave and Guided Wave Letters*, Vol. 10, No. 3, 92–93, 2000.
11. Kuo J.-T. and J. Shen, "A compact distributed low-pass filter with wide stopband," *Asia Pacific Microwave Conference*, Vol. 1, 330–333, 2001.
12. Hsieh, L. H. and K. Chang, "Compact elliptic-function low-pass filters using microstrip stepped-impedance hairpin resonators," *IEEE Trans. Microw. Theory Tech.*, Vol. 51, No. 1, 193–199, 2003.
13. Luo, S., L. Zhu, and S. Sun, "Stopband-expanded low-pass filters using microstrip coupled-line hairpin units," *IEEE Microwave and Wireless Components Letters*, Vol. 18, No. 8, 506–508, 2008.
14. Li, L., Z.-F. Li, and J.-F. Mao, "Compact lowpass filters with sharp and expanded stopband using stepped impedance hairpin units," *IEEE Microwave and Wireless Components Letters*, Vol. 20, No. 6, 310–312, 2010.
15. Lim, J.-S., C.-S. Kim, D. Ahn, Y.-C. Jeong, and S. Nam, "Design of low-pass filters using defected ground structure," *IEEE Trans. Microw. Theory Tech.*, Vol. 53, No. 8, 2539–2545, 2005.
16. Chen, J., Z.-B. Weng, Y.-C. Jiao, and F.-S. Zhang, "Lowpass filter design of hilbert curve ring defected ground structure," *Progress In Electromagnetics Research*, Vol. 70, 269–280, 2007.
17. Ting, S.-W., K.-W. Tam, and R. P. Martins, "Miniaturized microstrip lowpass filter with wide stopband using double equilateral U-shaped defected ground structure," *IEEE Microwave and Wireless Components Letters*, Vol. 16, No. 5, 240–242, 2006.
18. Zhang, J., B. Cui, S. Lin, and X.-W. Sun, "Sharp-rejection lowpass filter with controllable transmission zero using complementary split ring resonators (CSRRS)," *Progress In Electromagnetics Research*, Vol. 69, 219–226, 2007.
19. Ge, L., J. P. Wang, and Y.-X. Guo, "Compact microstrip lowpass filter with ultra-wide stopband," *Electronics Letters*, Vol. 46,

No. 10, 689–690, 2010.

20. Yang, M. H., J. Xu, Q. Zhao, L. Peng, and G. P. Li, "Compact, broad-stopband lowpass filters using SIRS-loaded circular hairpin resonators," *Progress In Electromagnetics Research*, Vol. 102, 95–106, 2010.
21. Sun, S. and L. Zhu, "Stopband-enhanced and size-miniaturized low-pass filters using high-impedance property of offset finite-ground microstrip line," *IEEE Trans. Microw. Theory Tech.*, Vol. 53, No. 9, 2844–2850, 2005.
22. Li, R., D. Kim, and C.-M. Choi, "Compact structure with three attenuation poles for improving stopband characteristics," *IEEE Microwave and Wireless Components Letters*, Vol. 16, No. 12, 663–665, 2006.
23. Yang, J.-P. and W. Wu, "Transmission characteristic research and application of parallel coupled-line loaded open-circuited resonator," *Journal of Microwaves*, Vol. 24, No. 3, 48–52, 2008 (in Chinese).
24. Ma, K. and K. S. Yeo, "New ultra-wide stopband low-pass filter using transformed radial stubs," *IEEE Trans. Microw. Theory Tech.*, Vol. 59, No. 3, 604–611, 2011.
25. Hsieh, M.-Y. and S.-M. Wang, "Compact and wideband microstrip bandstop filter," *IEEE Microwave and Wireless Components Letters*, Vol. 15, No. 7, 472–474, 2005.
26. Wu, Y., Y. Liu, S. Li, and C. Yu, "A simple microstrip bandpass filter with analytical design theory and sharp skirt selectivity," *Journal of Electromagnetic Waves and Applications,* Vol. 25, No. 8–9, 1253–1263, 2011.